Heterostructure iron selenide/cobalt phosphide film grown on nickel foam for oxygen evolution

Shuling Liu*, Yichuang Xing, Zixiang Zhou, Yifan Yang, Yvpei Li, Xuechun Xiao, Chao Wang*

Department of Chemistry and Chemical Engineering, Shaanxi Collaborative Innovation Center of Industrial Auxiliary Chemistry & Technology, Key Laboratory of Auxiliary Chemistry and Technology for Chemical Industry, Ministry of Education, The Youth Innovation Team of Shaanxi Universities, Shaanxi University of Science and Technology, Xi'an, Shaanxi 710021, P. R. China

*Corresponding Authors

E-mail address: shulingliu@aliyun.com

cwang@sust.edu.cn

1. Experimental

2. Instrumentation

3. X-ray photoelectron spectroscopy

4. X-ray diffraction

5. EDS

6. Electrochemistry

7. Activity comparison

8.TEM

9. References

1. Experimental

Chemicals

Cobalt(II) nitrate hexahydrate (Co(NO$_3$)$_2$·6H$_2$O; Guanghua Chemical Reagent; AR 98.0%), potassium hydroxide (KOH; Kermel Chemical Reagent; AR 85.0%), white phosphorous (P$_4$; Fuchen Chemical Reagent; AR), ethanol (C$_2$H$_5$OH; Rionlon Chemical Reagent; AR 99.7%), benzene (C$_6$H$_6$; Hushi Chemical Reagent; AR 99.5%), methanol (CH$_3$OH; Guanghua Chemical Reagent; AR 99.5%), ethylene glycol (C$_2$H$_6$O$_2$; Guanghua Chemical Reagent; AR 99.0%), acetone (C$_3$H$_6$O; Hushi Chemical Reagent; AR 99.5%), hydrochloric acid (HCl; Kelong Chemical Reagent; AR 38%), polyethylene glycol (HO(CH$_2$CH$_2$O)$_n$H; Damao Chemical Reagent; AR 99.0%), ferrous sulfate heptahydrate (FeSO$_4$·7 H$_2$O; Tianli Chemical Reagent; AR 99.0%), selenium dioxide (SeO$_2$; Macklin Chemical Reagent; AR 99.0%), sodium sulfate anhydrous (Na$_2$SO$_4$; Damao Chemical Reagent; AR 99.0%), potassium nitrate (KNO3; Hengxing Chemical Reagent; AR 99.0%), tetramethylammonium hydroxide pentahydrate (C$_4$H$_{13}$NO·5H$_2$O; Macklin Chemical Reagent; AR 97.0%), Ni foam (thickness 1.6 mm) were used as received unless stated otherwise. Doubly distilled water was used throughout the experiment.

2.Instrumentation

X-ray photoelectron spectroscopy (XPS) was carried out using a Kratos Axis Supra spectrometer at room temperature and ultra-high vacuum (UHV) conditions. The instrument was equipped with monochromatic Al Kα source 1486.6 eV (15 mA, 15 kV), and hemispherical analyser with hybrid magnetic and electrostatic lens for enhanced electron collection. Survey and detailed XPS spectra were acquired at normal emission with the fixed pass energy of 160 eV and 40 eV, respectively. All spectra were charge-corrected to the hydrocarbon peak set to 284.6 eV. The Kratos charge neutralizer system was used on all specimens. Data analysis was based on a standard deconvolution method using mixed Gaussian (G) and Lorentzian (L) line shape (G = 70% and L = 30%, Gaussian–Lorentzian product) for each component. Spectra were analyzed using CasaXPS software (version 2.3.16). X-ray diffraction (XRD) was acquired using (D8 ADVANCE, Bruker) diffractometer having Cu Kα (λ=1.54 Å) source. The instrument was operated at 30 mA current voltage and 40 kV. Field emission scanning electron microscope (S-4800, Hitachi, Japan) and transmission electron microscope (FEI-Tecnai G^2 F20) were used to observe the morphology of the catalyst. ICP-AES parameters are the following: forward power 1350 W, plasma gas flow rate 12.0 L min^{-1}, nebulizer gas flow rate 1.0 L min^{-1}, auxiliary gas flow rate 1.0 L min^{-1}, sample uptake speed 50 rpm with white/orange Tygon tubing. A concentric nebulizer was used with a cyclonic spray chamber. No internal standard correction was applied for ICP-AES analysis.

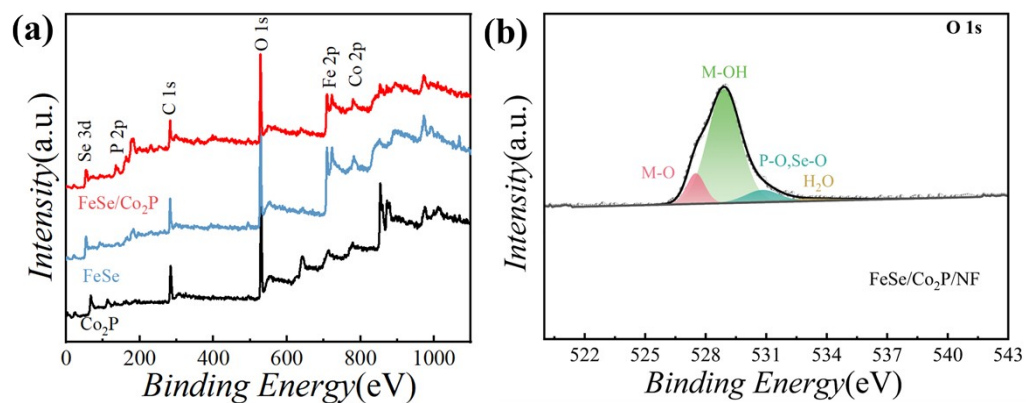## 3. X-ray photoelectron spectroscopy

Figure S1. (a) XPS survey spectra of the Co_2P/NF, $FeSe/NF$ and $FeSe/Co_2P/NF$; (b)

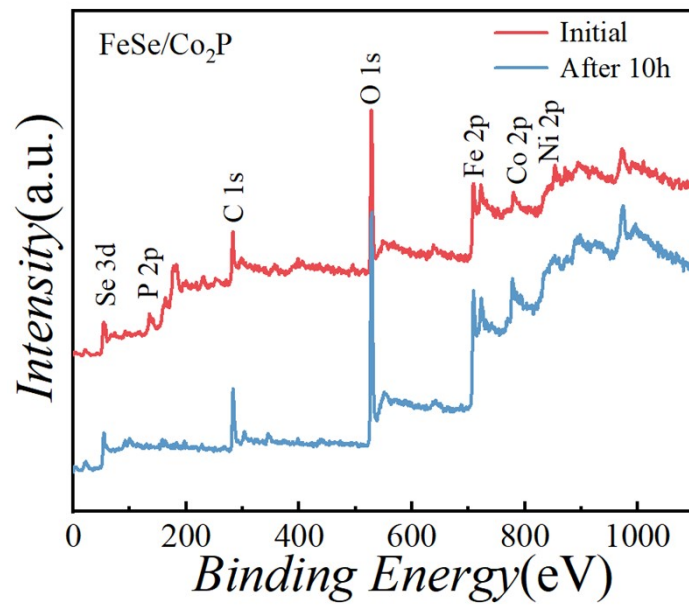Deconvoluted high-resolution XPS spectra of the O 1s region of $FeSe/Co_2P/NF$.

Figure S2. XPS survey spectra of the FeSe/Co$_2$P/NF after the long-term galvanostatic test.
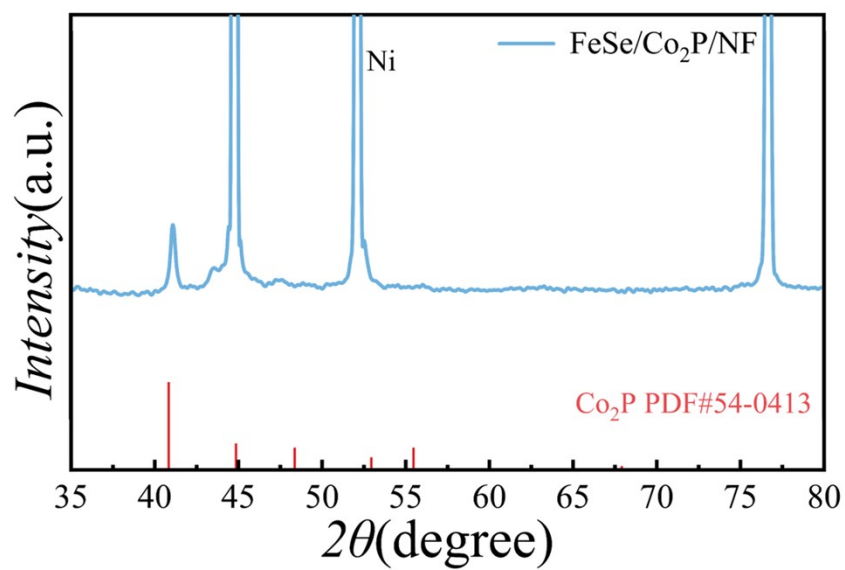
4. X-ray diffraction
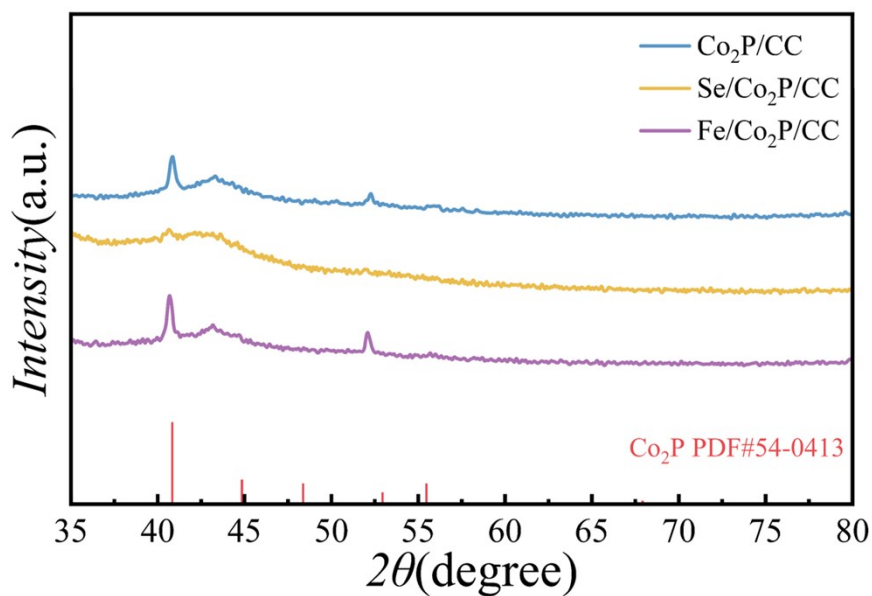

Figure S3. XRD pattern of FeSe/Co$_2$P/NF.

Figure S4. XRD patterns of Co$_2$P/CC, Se/Co$_2$P/CC and Fe/Co$_2$P/CC.
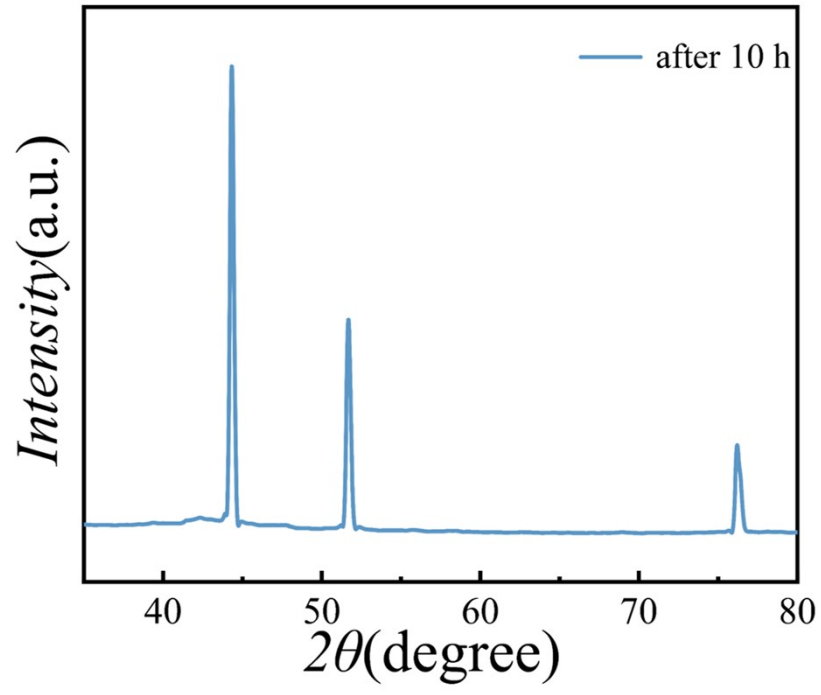
Figure S5. XRD patterns of FeSe/Co$_2$P/NF after the long-term galvanostatic OER test

5. EDS

Table S1. Contents of the deposited films

		Atomic Percentage (%)*			
		Co	Fe	P	Se
Co_2P	XPS	47.84	-	52.16	-
	EDS	64.66	-	35.34	-
FeSe	XPS	-	48.79	-	51.21
	EDS	-	56.52	-	43.48
FeSe/Co_2P	ICP- AES	29.90	6.65	56.96	6.46
	XPS	15.55	37.77	28.43	18.25
FeSe/Co_2P after 10h OER	XPS	32.58	67.42	-	-

6. Electrochemistry
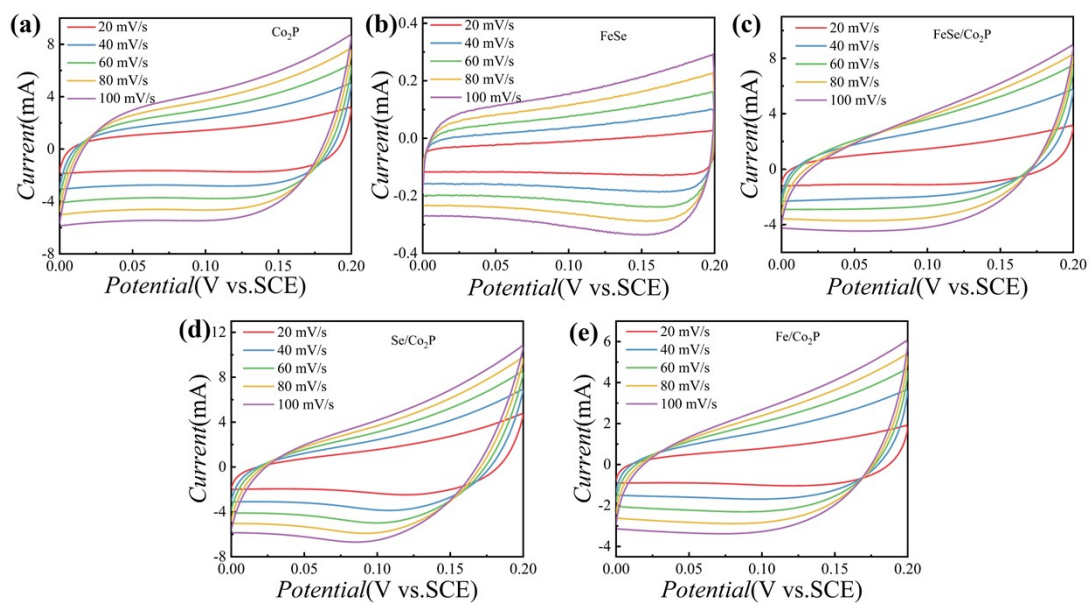
Figure S6. (a-e) CV of Co$_2$P/NF, FeSe/NF and X/Co$_2$P/NF (X = Se, Fe, FeSe) at different scan rates (20, 40, 60, 80, and 100 mV s^{-1}) in 0 - 0.2 V in 1 M KOH.
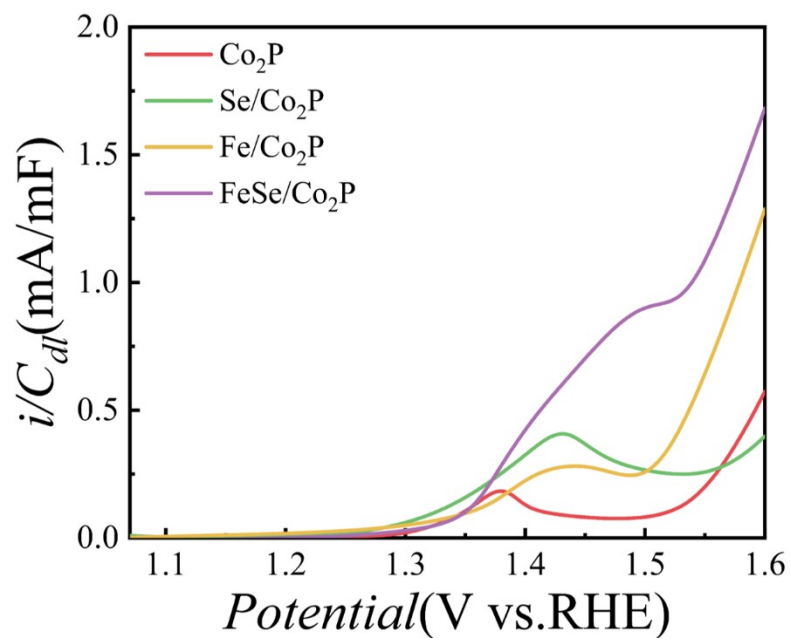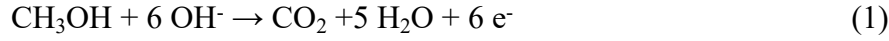
Figure S7. Plots of the OER current densities normalized to C_{dl}.

For methanol electrooxidation in alkaline solution,

$$CH_3OH + 6\ OH^- \rightarrow CO_2 + 5\ H_2O + 6\ e^- \tag{1}$$

the standard redox potential (E^o) is 0.02 V_{RHE}.

Assuming that the current-potential behavior follows the Butler-Vomer kinetics, and that at high overpotential, the cathodic current density is negligible, the current-potential relationship is described by Eq. 5,

$$j = j_0\ e^{\beta f \eta} \tag{2}$$

$$f = F/RT \tag{3}$$

where j is the current density, j_0 is the exchange current density, β is the transfer coefficient, η is the overpotential, and other variables have their standard meanings. By taking logarithm of Eq. 5, there is

$$\log j = \log j_0 + \alpha f \eta / 2.303 RT \tag{4}.$$

Therefore, by plotting the $\log j$ vs. η plot, the j_0 can be acquired from the intercept.

The j_0 of MOR for Co_2P, $FeSe/Co_2P$ are 2.29×10^{-12} mA cm^{-2} and 7.08×10^{-16} mA cm^{-2}, respectively. These values are significantly smaller than the Pt based electrocatalysts for MOR [1,2].
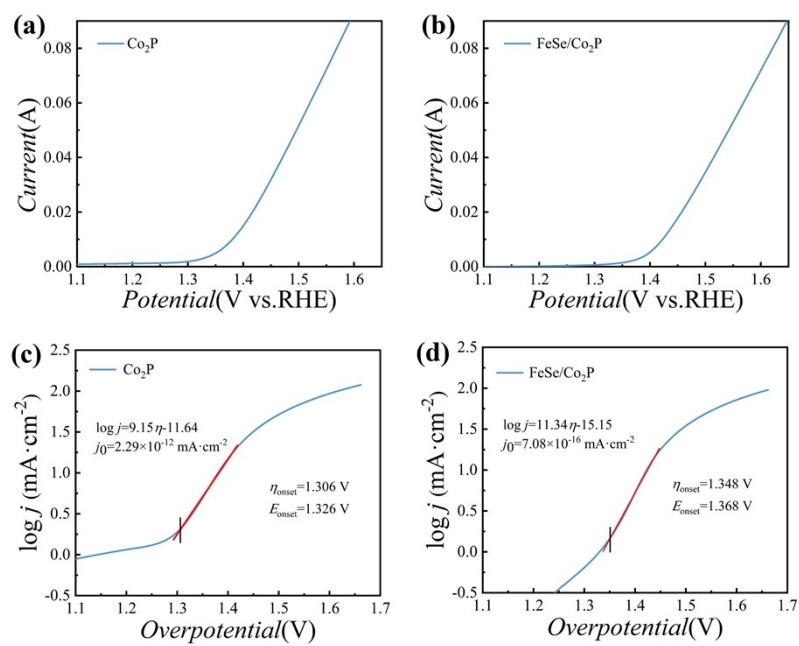
Figure S8. The LSV of the Co_2P/NF and $FeSe/Co_2P$ /NF electrodes in 0.5 M CH_3OH + 1 M KOH (scan rate 5 mV s^{-1})
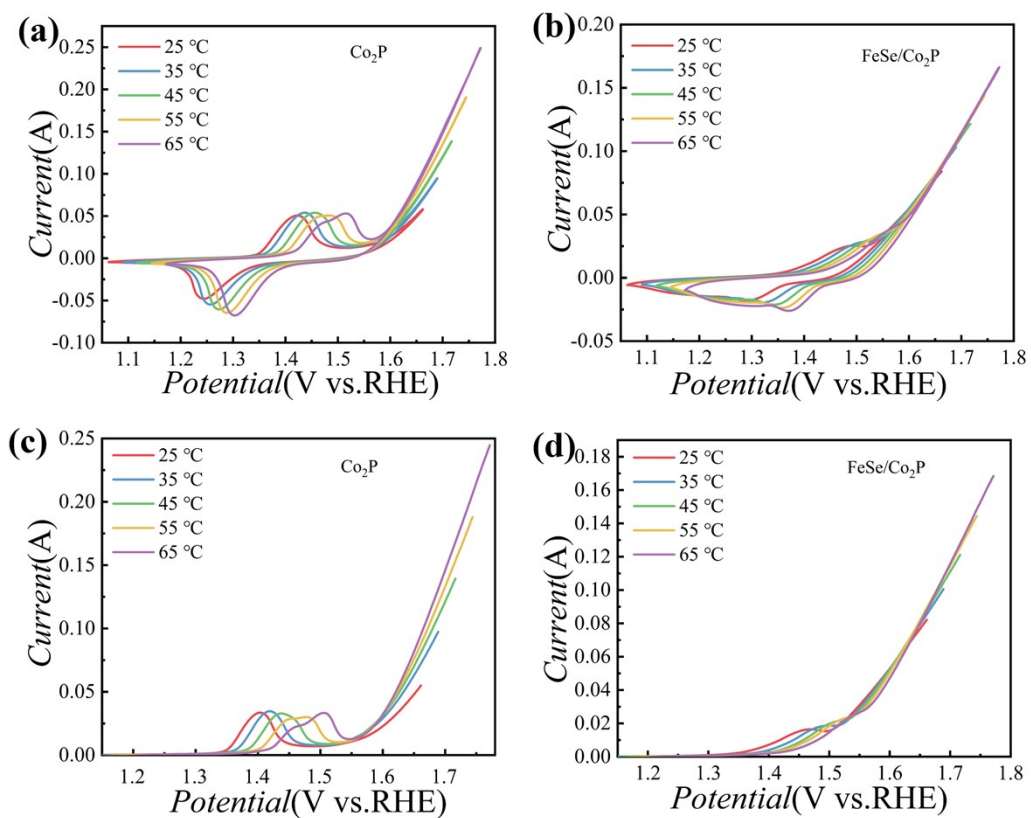
Figure S9. The CV and LSV of the (a, c) Co_2P/NF and (b, d) FeSe/Co_2P /NF at different temperatures in 1 M KOH at scan rate 5 mV s^{-1}.
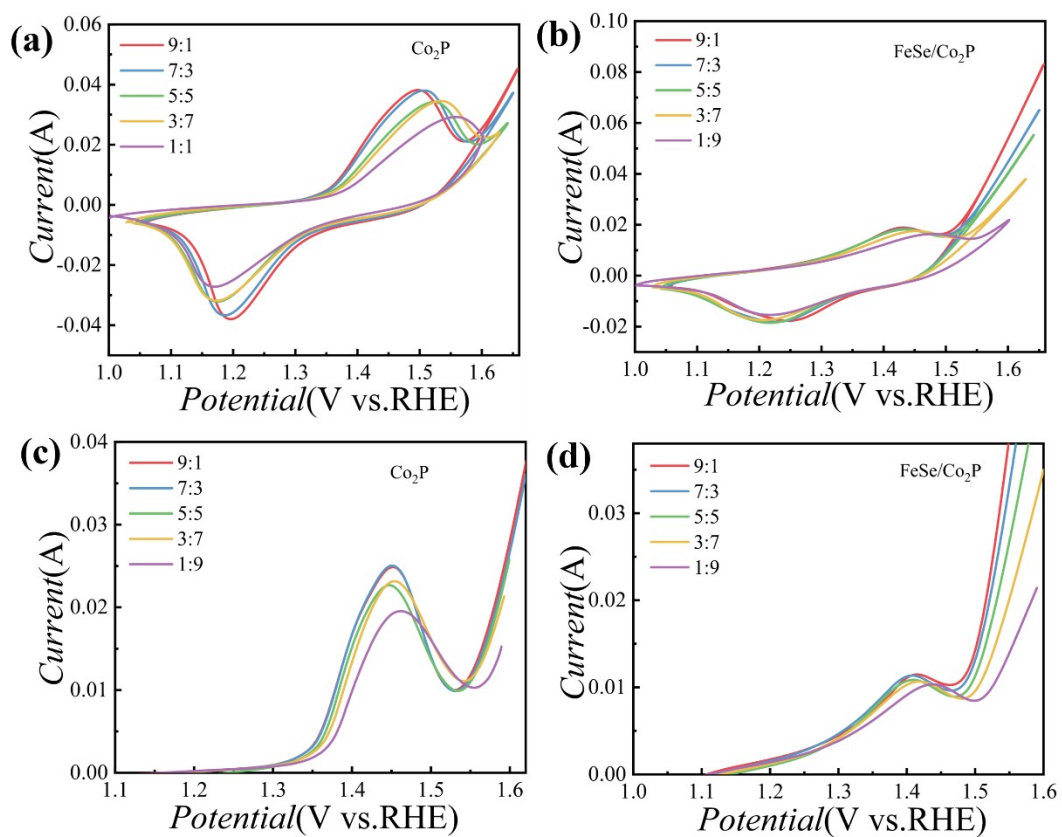
Figure S10. The CV and LSV of the (a, c) Co_2P/NF and (b, d) FeSe/Co_2P /NF in different pH solutions (x M KOH + (1-x) M KNO_3, pH=13.84, 13.72, 13.57, 13.35, and 12.9) at scan rate 5 mV s^{-1}.
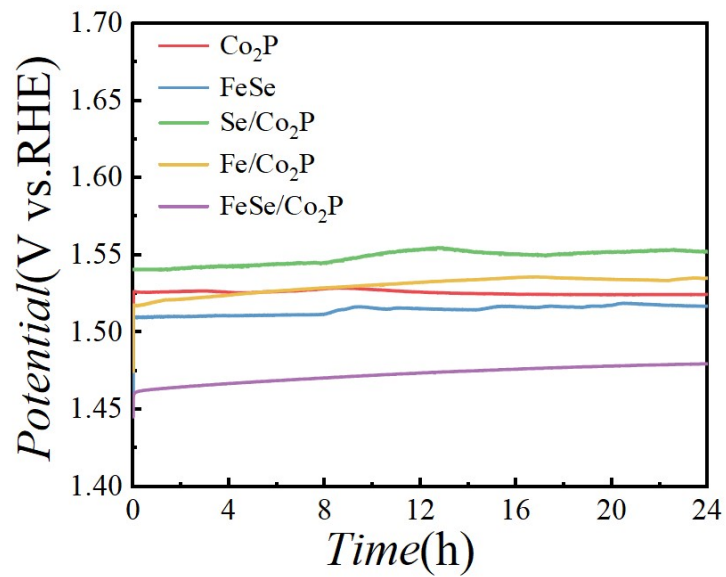
Figure S11. The 10 mA cm^{-2} galvanostatic test of the Co$_2$P/NF, FeSe/NF and

X/Co$_2$P/NF (X = Se, Fe, FeSe) in 1 M KOH.

Table S2. EIS fitting results

	Rs / Ω	Error / %	R_{CT} / Ω	Error / %
Co$_2$P	2.53	0.31	2.26	0.78
FeSe	2.58	0.19	1.65	1.62
Se/Co$_2$P	2.56	0.16	2.01	1.29
Fe/Co$_2$P	2.58	0.53	1.89	2.55
FeSe/Co$_2$P	2.50	0.19	1.51	0.75
FeSe/Co$_2$P after 10 h OER	2.58	0.24	1.85	1.01

7. Activity comparison

Table S3. OER activity comparison in alkaline solutions

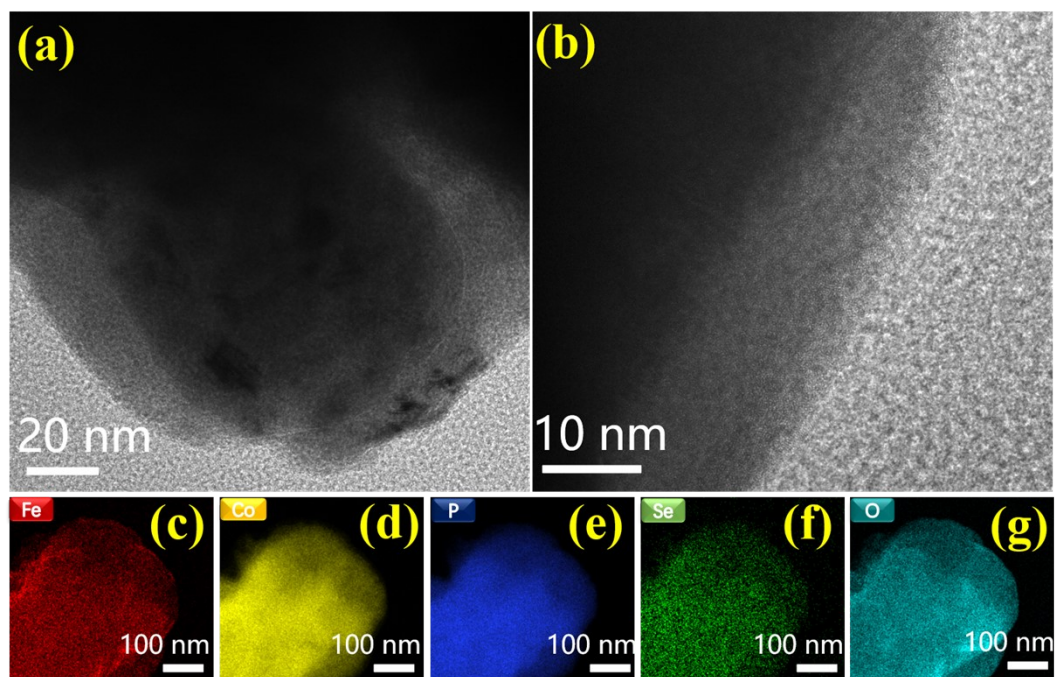| Catalysts	Loadings/ mg cm^{-2}	η at 10 mA cm^{-2}	Tafel slope/ mV dec^{-1}	References
FeSe/Co$_2$P/NF	3.5	235 mV	65.6	This work
CoP–TiOx	0.2	337	72.1	[3]
CoP/CeO$_2$	0.06	224	90.3	[4]
Fe$_{0.45}$Co$_{0.55}$P/NiP@CC	1.6	247 mV	56	[5]
Co$_2$P@NC–Fe$_2$P	0.5	260	41	[6]
Ag@CoxP	-	310	76.4	[7]
CoP@FeNiP	1.92	283 at 100 mA cm^{-2}	31.8	[8]
CuO-FR@CoP/CF	9.2	290 at 50 mA cm^{-2}	56	[9]
Fe-CoP/CoO	0.285	219	52	[10]
FeCo-P/C	-	360	50.1	[11]
CoP@CoFe-LDH/NF	-	240 at 40 mA cm^{-2}	69.2	[12]

8. TEM

Figure S12. (a) TEM and (b) HRTEM images of FeSe/Co$_2$P/NF after the long-term

galvanostatic OER test; (c-g) elemental mapping of FeSe/Co$_2$P/NF.

9. References

[1]   Z Merati, JB Parsa, R Babaei-Sati. Electrochemically synthesized polypyrrole/MWCNTs-Al2O3 ternary nanocomposites supported Pt nanoparticles toward methanol oxidation. *int j hydrogen energ*. 2018;43(45):20993-21005.

[2]   L Chen, X Liang, D Wang, Z Yang, C-T He, W Zhao, J Pei, YJAAM Xue. Platinum–Ruthenium Single Atom Alloy as a Bifunctional Electrocatalyst toward Methanol and Hydrogen Oxidation Reactions. *ACS Appl Mater Inter*. 2022;14(24):27814-27822.

[3]   Z Liang, W Zhou, S Gao, R Zhao, H Zhang, Y Tang, J Cheng, T Qiu, B Zhu, C Qu. Fabrication of hollow CoP/TiOx heterostructures for enhanced oxygen evolution reaction. *Small*. 2020;16(2):1905075.

[4]   M Li, X Pan, M Jiang, Y Zhang, Y Tang, G Fu. Interface engineering of oxygen-vacancy-rich CoP/CeO2 heterostructure boosts oxygen evolution reaction. *Chem Eng J*. 2020;395:125160.

[5]   BZ Desalegn, HS Jadhav, JG Seo. Interface modulation of a layer-by-layer electrodeposited Fe x Co (1− x) P/NiP@ CC heterostructure for high-performance oxygen evolution reaction. *Sustain Energ Fuels*. 2020;4(4):1863-1874.

[6]   Y-J Tang, L You, K Zhou. Enhanced Oxygen Evolution Reaction Activity of a Co2P@ NC–Fe2P Composite Boosted by Interfaces Between a N-Doped Carbon Matrix and Fe2P Microspheres. *ACS appl mater inter*. 2020;12(23):25884-25894.

[7]   Y Hou, Y Liu, R Gao, Q Li, H Guo, A Goswami, R Zboril, MB Gawande, X Zou. Ag@ Co x P core–shell heterogeneous nanoparticles as efficient oxygen evolution

reaction catalysts. *ACS Catal*. 2017;7(10):7038-7042.

[8]   J Wang, C Chen, N Cai, M Wang, H Li, F Yu. High topological tri-metal phosphide of CoP@ FeNiP toward enhanced activities in oxygen evolution reaction. *Nanoscale*. 2021;13(2):1354-1363.

[9]   Q Zhou, T-T Li, F Guo, Y-Q Zheng. Construction of hierarchically structured CuO@ CoP anode for efficient oxygen evolution reaction. *ACS Sustain Chem Eng*. 2018;6(9):11303-11312.

[10]   X Hu, S Zhang, J Sun, L Yu, X Qian, R Hu, Y Wang, H Zhao, J Zhu. 2D Fe-containing cobalt phosphide/cobalt oxide lateral heterostructure with enhanced activity for oxygen evolution reaction. *Nano Energy*. 2019;56:109-117.

[11]   W Hong, M Kitta, Q Xu. Bimetallic MOF-derived FeCo-P/C nanocomposites as efficient catalysts for oxygen evolution reaction. *Small Methods*. 2018;2(12):1800214.

[12]   H Feng, X Sun, X Guan, D Zheng, W Tian, C Li, C Li, M Yan, Y Yao. Construction of interfacial engineering on CoP nanowire arrays with CoFe-LDH nanosheets for enhanced oxygen evolution reaction. *FlatChem*. 2021;26:100225.